DESIGN AND OPTIMIZATION OF SPHERICAL LENS ANTENNAS INCLUDING PRACTICAL FEED MODELS

M. Huang, S. Yang*, W. Xiong, and Z. Nie

School of Electronic Engineering, University of Electronic Science and Technology of China (UESTC), Chengdu 611731, China

Abstract—A novel approach for the design and optimization of spherical lens antennas (SLAs) including practical feed model (PFM) is proposed. The vector spherical wave function expansions (VSWE) combined with differential evolution (DE) algorithm is adopted for the optimal design of SLAs. Moreover, the near-field aperture distributions of a Ku band dielectric loaded horn feed and a Ka band corrugated horn feed were obtained using the full wave simulation and were then taken into account in the DE optimization. The performances of the optimized 2-layer design are compared with previous works, higher directivity is obtained. Additionally, the radiation characteristics of an optimized SLA are presented, and numerical results of a 650 mm diameter 2-layer hemispherical lens antenna (HLA) with ground plane are compared to the experimental results, and good agreements are obtained. An investigation of the influence of the various lens-to-feed distances as well as aperture sizes of SLA on the aperture efficiency for a 2-layer design is also proposed.

1. INTRODUCTION

Lens antennas (LAs) often have many attractive features such as the focusing properties, multiple beams, broadband behavior and very wide scan coverage without scanning losses. These features make LAs as attractive choices for various applications including radar cross-section (RCS) enhancers [1–3], satellite communication systems [4], automotive radars [5], and imaging systems at millimeter waves [6–9]. In the past decades, many analysis methods [10–17] and fabrication techniques [18–24] for LAs have been developed. For instance,

J. Thornton proposed a 236 mm diameter 2-layer hemispherical lens antenna (HLA) with ground plane using a Rexolite inner core and a polyethylene outer layer, which offers 35.1 dBi gain at 28 GHz [15], yet the physical aperture size is relatively small. Moreover, most of the previous works usually design spherical lens antennas (SLAs) with ideal primary sources models, such as the point source models, incident plane waves [11], end-fire dipoles [14, 15], or open-ended waveguide [16], which are inaccurate for the description of practical feed model (PFM). Taking into account the PFM in the SLA optimal design is rarely seen. B. Fuchs studied the scattering by SLAs fed by any real source and firstly quantized lens reactions to the feed [17]. In practical applications, the feed is usually an aperture antenna, and it is necessary to consider the spillover efficiency and uniformity of the amplitude distribution of the feed pattern over the SLA. Similar to the design of parabolic reflector antennas, the aperture efficiency of an SLA depends on the number of layers, dielectric losses, spillover efficiency and taper efficiency. For a given size of lens, the optimal SLA parameters and lens-to-feed distance should be determined to obtain a compromise between spillover and taper efficiency. Meanwhile, minimum number of layers of lens is preferred for practical implementations, due to the reduced cost of fabrication and the minimized effect of the air-gap between each two layers. Thus, the design of a high performance SLA with a smallest number of layers and taking into account the PFM become the motivation of this study.

Compared to previous studies presented in [10–16], a new approach for the optimal design of a SLA, taking into account the full-wave simulated aperture near-field distributions of PFM for two Ku/Ka feed horns, is described in this paper. This is especially feasible for the optimal design of even electrically large size SLAs,
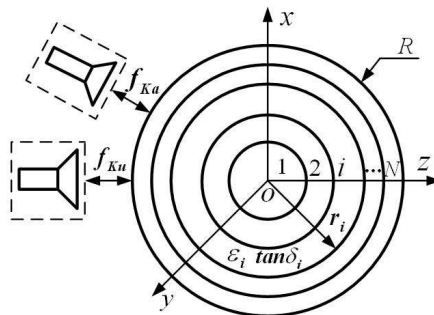

Figure 1. Geometry of an N-layer SLA fed by Ku/Ka horns.

since the full wave simulation of the entire lens-feed antenna system becomes unrealistic in each iteration of the optimization. It can be used to precisely predict the radiation characteristics of the lens antenna with feed. The vector spherical wave function expansions (VSWE) combined with differential evolution (DE) algorithm is adopted to fulfill this target. Then the convergence performance of DE algorithm is also presented for the optimized SLA. The performances of the optimized 2-layer design are compared with previous works, higher directivity is obtained. Numerical and Measured performances of a 650 mm diameter 2-layer SLA are also presented to show the validity of this study. Finally, an investigation of the influence of the various lens-to-feed distances as well as aperture sizes of SLA on the aperture efficiency for a 2-layer design is also proposed.

2. THEORETICAL ANALYSIS

An N-layer SLA of radius R illuminated by practical feed models of the Ku and Ka band horns is depicted in Figure 1. The variables r_i, ε_i and $\tan\delta_i$ are the outer radius, permittivity and dielectric loss of the ith layer, respectively, and f is the lens-to-feed distance. The near-field distributions of the facets of the virtual box enclosing the feed can be obtained by any 3D full wave simulation software. Compared to the radiation aperture of the feed horn, the field on other surfaces constitutes a relatively small component for radiation characteristics of the feed. For simplicity, the near-field distribution of radiation aperture of the feed horn is extracted and discretized into squares of $0.1\lambda \times 0.1\lambda$. The corresponding equivalent electromagnetic currents are $J_s = \hat{n} \times H$ and $M_s = E \times \hat{n}$, where $\hat{n}$ denotes the unit outer normal vector on the radiation aperture of the feed horn. The $\mathbf{E}$ and $\mathbf{H}$ denote the electric and magnetic fields of the near field plane, respectively.

The horn radiation aperture can be synthesized from a set of equivalent infinitesimal current elements. When using an infinitesimal electric current element as a feed, the field in ith layer can be written as an expansion of the incoming and outgoing traveling spherical wave modes $\mathbf{m}$ and $\mathbf{n}$ [13],

$$H_i = \sum_{n=1}^{\infty} \left\{ a_n^i m_{e1n}^{(1)} + b_n^i n_{o1n}^{(1)} + c_n^i m_{e1n}^{(3)} + d_n^i n_{o1n}^{(3)} \right\} \qquad (1)$$

$$E_i = \frac{k_i}{j\omega\varepsilon_i} \sum_{n=1}^{\infty} \left\{ a_n^i n_{e1n}^{(1)} + b_n^i m_{o1n}^{(1)} + c_n^i n_{e1n}^{(3)} + d_n^i m_{o1n}^{(3)} \right\} \qquad (2)$$

where n is the mode number, the superscripts (1) and (3) are the spherical Bessel function of the first kind and Hankel function of

the second kind, respectively. The coefficients a_n, b_n, c_n, and d_n, weighting the contribution of each mode in ith layer, are derived from the boundary conditions at each interface. The number of the terms N_{mode} needed in modal expansions (1) and (2) is proportional to the maximum dimension of the SLA. The value of N_{mode} is selected as $N_{\mathrm{mode}} > kR + 20$, where k is the wave number. The choice of the number 20 is a rule of thumb and depends on the maximum dimension of SLA and the convergence of the electric field.

The radiation characteristic of a lens-feed antenna system is modeled by using superposition of the fields of the elementary radiators with the appropriate coordinate transformations. Thus, the total field of the lens-feed antenna system is the integral of Green functions on the radiation aperture of the feed, given by

$$E_{total} = \int_s (G_e \cdot J_s + G_m \cdot M_s) ds \tag{3}$$

$\mathbf{G}_e$ and $\mathbf{G}_m$ are electric and magnetic current Green functions of the spherically symmetric geometry corresponding to infinitesimal current elements. $\mathbf{G}_e$ can be derived from (1) and (2), and $\mathbf{G}_m$ is obtained by invoking duality.

Many global optimization techniques, such as the particle swarm optimization (PSO) [16], genetic algorithm (GA) [25], ant colony optimization (ACO) [26], and DE algorithm [27–31] have recently been successfully applied to electromagnetic problems. In this article, DE algorithm is applied in the design of an SLA to achieve optimal radiation characteristics. It operates on a population with N_{pop} individuals and each individual is a symbolic representation of the N_{par} optimization parameters. It follows a general procedure of an evolutionary algorithm using three kinds of operators: mutation, crossover, and selection. The mutation generates a mating partner as follows:

$$x^{M,j} = x^{n,opt} + \beta(x^{n,p_1} - x^{n,p_2}), \ j \neq p_1, \ j \neq p_2, \ \text{and} \ p_1 \neq p_2 \tag{4}$$

where M is mating pool, n is the generation index of the parent population, j, p_1, p_2 are individual indexes of parent population, and p_1, p_2 are randomly selected. opt denotes the optimal individual of parent population. The real constant β is the control factor (mutation intensity). Then crossover operation is introduced to generate the population of candidates (children individuals), given by

$$(x^{C,j})_i = \begin{cases} (x^{M,j})_i, & \gamma \leq p_{\mathrm{cross}} \\ (x^{n,j})_i, & \text{otherwise} \end{cases} \tag{5}$$

where C is the children population, $(x^{c,j})_i$ denotes the ith gene (here optimization parameter) of the jth children individual, γ is a real

random number in the range [0, 1] and p_{cross} is the probability of crossover. Finally, the selection (competition) determines that the child or its parent becomes a member of next generation. In this way, all individuals in the current generation are as good as or better than those in the previous generation. As usual, the stopping criterion is either a cost function threshold or a maximum number of iterations.

The proper choices of the parameters (N_{pop}, β, p_{cross}) and the objective function are crucial to the convergence of the minimization problem. The initial population should be spread as much as possible over the objective function surface. For many applications, $N_{\text{pop}} = 10N_{\text{par}}$ is a good choice, β and p_{cross} are usually chosen $\in [0.5, 1]$ and $[0.8, 1]$, respectively [27]. However, in some applications [29, 31], it is also effective to set $N_{\text{pop}} = 5N_{\text{par}}$ to speed up the convergence rate. The specific parameter value is set by the user for different conditions. According to [29], the population size is set as $N_{\text{pop}} = 5N_{\text{par}}$, the mutation intensity and crossover probability are $\beta = 0.6$ and $p_{\text{cross}} = 0.9$, respectively, for the following examples.

In this paper, DE algorithm is applied to maximize the gain and aperture efficiency of a given dimension SLA both for Ku and Ka bands. The cost function is defined by

$$F^{(n)} = w_1 \cdot \left| \eta_{0\text{Ku}} - (dir_{\text{Ku}}/g_{0\text{Ku}})^{(n)} \right| + w_2 \cdot \left| \eta_{0\text{Ka}} - (dir_{\text{Ka}}/g_{0\text{Ka}})^{(n)} \right| \quad (6)$$

where n denotes the nth generation of the evolution, η_0 represents the objective aperture efficiency, dir represents the calculated directivity of the SLA, g_0 represents the directivity of a uniformly illuminated constant phase aperture, thus, dir/g_0 is the calculated aperture efficiency. By properly selecting the weighting factors w_1 and w_2, one can effectively control the gain of SLA both for Ku and Ka bands. The weighting factors are continuously adjusted until the minimization is going to converge.

The optimization vector $\mathbf{v}$ is defined by $\mathbf{v}=\{d_i, \varepsilon_i, \tan\delta_i, f_{\text{Ku}}, f_{\text{Ka}},$ for $i = 1, 2, \ldots, N\}$, where d_i denotes ith layer thickness. The practical near-field aperture distributions of Ku/Ka horns were also taken into account in the DE optimization. The structural parameters of SLA should satisfy the following equation

$$\begin{cases} d_1 + d_2 + \ldots + d_N = R \\ r_1 = d_1 > d_2, d_3, \ldots, d_N \\ \varepsilon_{i+1} = \varepsilon_i - \Delta\varepsilon_{i+1} \geq 1, \text{ for } i = 1, 2, \ldots, N-1 \\ \Delta\varepsilon_{i+1} \geq \sigma_p, \text{ for } i = 1, 2, \ldots, N-1 \\ f_{\text{ku}}, f_{\text{ka}} \in [0, 0.5R] \end{cases} \quad (7)$$

In fact, the thickness of each layer can be allowed to change arbitrarily in the range $(0, R)$. However, the larger search range of parameters

is time consuming. It is well known that the quality of focusing is inversely proportional to the projected area of the spherical layer. The innermost layer d_1 should be a little thicker than outer layers. To achieve a fast optimum design, the constraint on the layer d_1 is imposed. $\Delta\varepsilon_{i+1}$ is the increment permittivity, and σ_p represents the control precision of permittivity for each layer, especially for the composite foam materials for Luneberg lens. The available low loss materials (ε_i: $1.0 \sim 5.0$) can also be picked up from the database. The search ranges of f_{Ku} and f_{Ka} are selected as $[0, 0.5R]$ to obtain a compromise between spillover and taper efficiency. When r_{N-1} is greater than R, or ε_N is smaller than 1.0, the individual is abandoned. The design procedure of SLA is summarized in Figure 2.

Theoretically, the HLA with ground plane has the same radiation aperture as an SLA, with advantages such as the relatively low-profile and easy to be mounted on vehicles. However, due to the shadowing effects caused by the presence of the feed, the radiation aperture of HLA is slightly smaller than SLA. The field reflected from the ground plane dominates the main lobe region of HLA, while those radiated directly from feed and lens is small and comprises part of the back lobe region [15]. Thus, the gain of HLA can be readily predicted by the SLA.
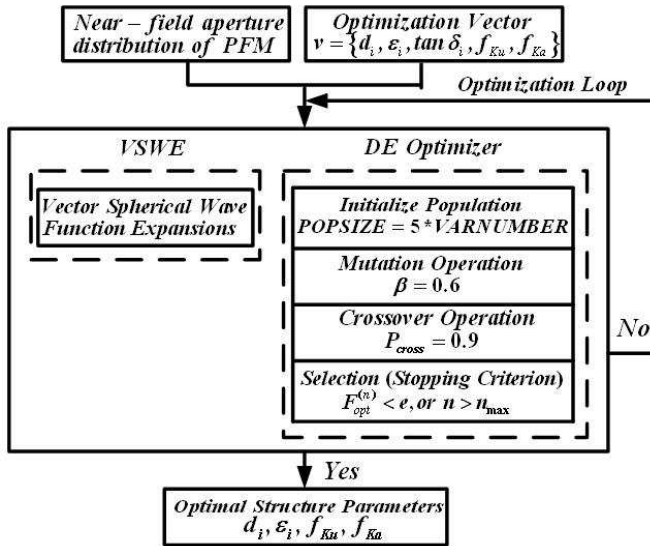

Figure 2. Flowchart describing the design procedure of SLA.

3. DESIGN AND EXPERIMENTAL VALIDATIONS

3.1. Numerical Simulation and Comparison

To demonstrate the capability of the design procedure and make a fair comparison with a 2-layer lens design in [14], an example of a 2-layer 30λ diameter SLA (without consideration of dielectric losses) is considered. The permittivity ε_i is allowed to change between $1.0 \sim 5.0$, the thickness of the inner core is changed between $7.5 - 15\lambda$, and the search range of f is selected as $[0, 7.5\lambda]$. The practical near-field aperture distribution of a corrugated horn is also taken into account in the DE optimization. The design parameters and optimal results are shown in Table 1. The radiation performance of the 30λ diameter optimized 2-layer SLA is plotted in Figure 3. The optimized 2-layer SLA offers gain of 37.92 dBi ($\eta_{ap} = 69.7\%$) with sidelobe level

Table 1. Design parameters and optimal results of 2-layer 30λ diameter SLA.

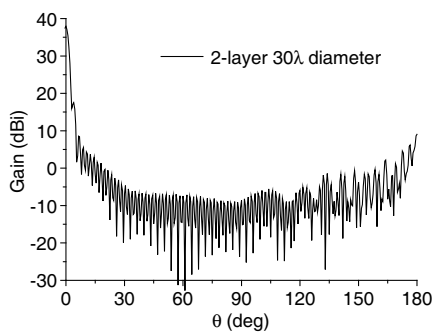| Parameters	Design parameters	Optimized results
Layer permittivity ε_i	$1 \leq \varepsilon_i \leq 5$, for $i = 1, 2$	3.072, 1.682
Layer thickness d_i (λ)	$7.5\lambda \leq d_1 \leq 15\lambda$, $d_2 = 30\lambda - d_1$	14.755, 0.245
Lens-to-feed distance (λ)	$0 \leq f \leq 7.5\lambda$	0
Gain (dBi)	37.92 dBi ($\eta = 69.7\%$)	

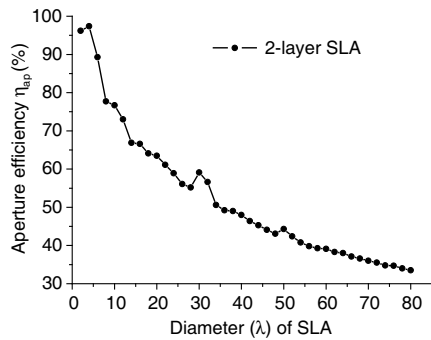**Figure 3.** Gain pattern of the 30λ diameter optimized 2-layer SLA.

Figure 4. Influence of the aperture size of the lens on the aperture efficiency η_{ap} for an optimized 2-layer SLA.

(SLL) about -20.43 dB. Compared to the previous work (37.48 dBi, $\eta_{ap} = 63\%$, SLL $= -13.73$ dB) [14], this optimal design helps the increment in the gain of SLA by 0.44 dB, and also has a 6.7 dB improvement in SLL.

An investigation of the influence of various aperture sizes of SLA on the aperture efficiency η_{ap} for the optimized 2-layer design is also presented in Figure 4. It shows the frequency dependence of the SLA. As the lens becomes larger, i.e., by increasing the operating frequency, the phase errors at the radiation aperture of lens increase, thus the aperture efficiency decreases more quickly for the 2-layer design. When the diameter of 2-layer SLA is larger than 56λ, the η_{ap} is less than 40%, as observed in Figure 4. The higher aperture efficiency could be expected for the SLA with more number of layers.

3.2. Experimental Validation and Discussion

The aforementioned method is applied in the design of an SLA to achieve optimal gain both at Ku and Ka bands. Of particular interest to this example is to choose from a mall list of existing and machinable industrial materials which have low dielectric losses and known permittivities, and design a high performance SLA for Ku and Ka bands with a smaller number of layers. Only a few materials ($\tan \delta_i$ about $3 \sim 7 \times 10^{-4}$) are available for us, such as the polyethylene, polystyrene, polypropylene, and polytetrafluoroethylene (PTFE) et al. The practical feed models of a Ku band dielectric loaded horn (linear polarization) and a Ka band corrugated horn (circular polarization) are shown in Figure 5. The near-field aperture distributions of Ku/Ka horns were obtained using the CST Microwave Studio (Figure 6) and were then taken into account in the DE optimization procedure. The

Figure 5. Photograph of the dielectric loaded horn (Ku band, linear polarization) and the corrugated horn (Ka band, circular polarization).
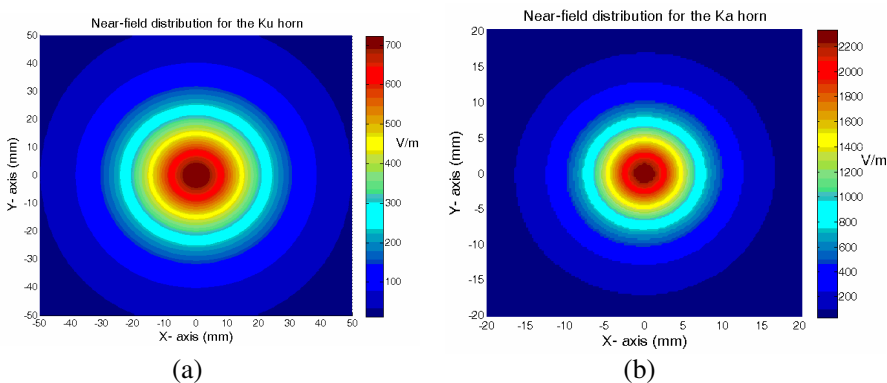
Figure 6. Near-field aperture amplitude distributions for the Ku and Ka horns, (a) Ku horn at 12.5 GHz, (b) Ka horn at 30 GHz.
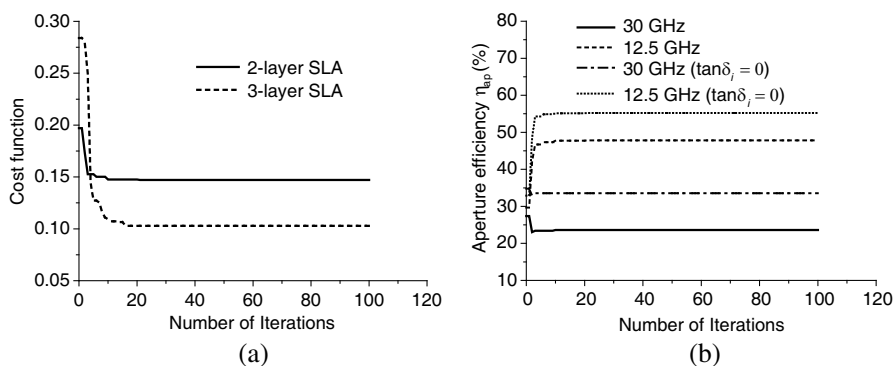

Figure 7. The convergence performance of the DE algorithm, (a) cost functions of 2-layer/3-layer SLAs, (b) aperture efficiency of 2-layer SLA.

-10 dB beam width of Ku and Ka band horns are $93.6°$ and $91°$, respectively. The Ku band horn has cross-polarization isolation about 40.2 dB with directivity of 11.67 dBi at 12.5 GHz. The Ka band horn has axial ratio less than 0.86 dB with directivity of 11.74 dBi at 30 GHz. The 2-layer/3-layer SLAs with a prescribed diameter of 650 mm are investigated. Due to the fixed permittivities and losses of existing materials, only the thickness of each layer and lens-to-feed distances can be optimized ($\mathbf{v} = \{d_i, f_{Ku}, f_{Ka}, \text{ for } i = 1, 2, \ldots, N\}$) in the lens design. However, the aperture efficiency is related to permittivity and losses of materials, the objective aperture efficiencies of SLA for Ku

Table 2. Gain of optimized 2-layer/3-layer SLAs for Ku and Ka bands.

Parameters		3-layer SLA	2-layer SLA
Materials		polystyrene, polyethylene, PTFE	polyethylene, PTFE
Layer permittivity ε_i		2.59, 2.32, 2.08	2.32, 2.08
$\tan\delta_i$ (10^{-4})		4.9, 6.5, 3.4	6.5, 3.4
Layer thickness d_i (mm)		275, 19, 31	296, 29
Lens-to-feed distance (mm)		$f_{\mathrm{ku}} = 19\,\mathrm{mm}$, $f_{\mathrm{ka}} = 47\,\mathrm{mm}$	$f_{\mathrm{ku}} = 57\,\mathrm{mm}$, $f_{\mathrm{ka}} = 86\,\mathrm{mm}$
Gain (dBi)	12.5 GHz	35.8	35.4
	30 GHz	40.7	39.84

Figure 8. A 650 mm diameter 2-layer HLA under the planar near-field measurement system.

and Ka bands are chosen as 60% and 40%, respectively. The weighting factors w_1 and w_2 are 0.6 and 0.4, respectively. Figure 7 shows the convergence performance of the DE algorithm for 2-layer/3-layer SLAs. It takes less than 28 generations (about 41.4 minutes) to converge into an optimum solution. The resulting objective function $F^{(n)}$ is 0.14717 for the 2-layer design. The optimized 2-layer/3-layer SLAs can offer above 35 dBi gain both at Ku and Ka bands (Table 2).

By compromising between performance and manufacture cost, a 650 mm diameter 2-layer HLA with a 990 mm ground plane was fabricated (Figure 8), using a polyethylene inner core (ε_r: 2.29 ∼ 2.38, core radius: 296 mm) and a polytetrafluoroethylene (PTFE) outer layer (ε_r: 2.04 ∼ 2.15). The optimal f_{Ku} and f_{Ka} are

57 mm and 86 mm, respectively. The uncertainty of gain is about ± 0.3 dBi within the accuracy ranges of material permittivity. The corresponding spillover efficiencies are about 1.21% and 3.72% at 12.5 GHz and 30 GHz, respectively. The optimized 2-layer SLA has an aperture efficiency of about 47.8% and 23.6% at 12.5 GHz and 30 GHz, respectively. On the other hand, for a conventional 2-layer uniform Luneberg lens antenna (LLA) with the same dimensions and dielectric losses, the corresponding aperture efficiencies are only 15.8% and 10.7%, respectively. Thus, it is found that the antenna efficiency is greatly improved as compared to that of the conventional LLA. When dielectric losses are neglected, the optimized 2-layer SLA has aperture efficiencies up to 55.2% and 33.6% at 12.5 GHz and 30 GHz, respectively. The relatively lower aperture efficiencies obtained here are mainly due to the limited availability of the dielectric materials and dielectric losses at high frequencies, consequently the number of layers of the SLA is only 2. As observed in Figure 4, the relatively lower aperture efficiencies for the 2-layer 650 mm diameter SLA obtained here is reasonable, due to the electrically large size for the 2-layer design (about 65λ diameter, especially at 30 GHz), the limited availability of the dielectric materials and dielectric losses at high frequencies.

Figure 9 presents the E-plane patterns of the SLA at 12.5 GHz. Patterns of SLA simulated by VSWE and CST are in good agreements, except for some negligible discrepancies at the back lobe region, which is due to the truncation errors of near-field distribution at the aperture of the feed horn. The 2-layer HLA model illuminated by the Ku band horn with an elevation angle of 45° (respective to the normal direction of the ground plane) is simulated by CST. The gain patterns of the
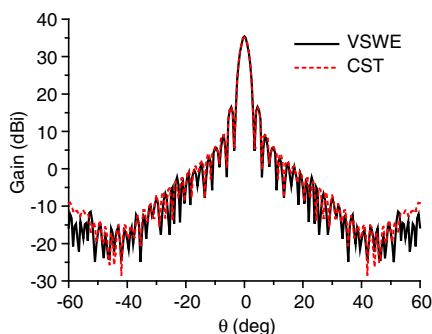

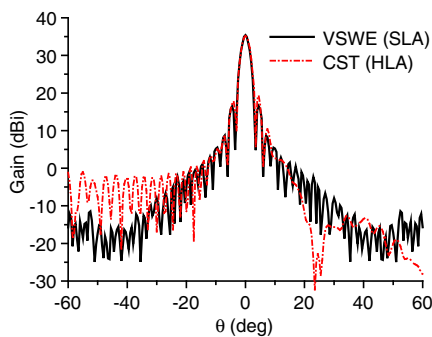**Figure 9.** Simulated E-plane patterns of SLA at 12.5 GHz.

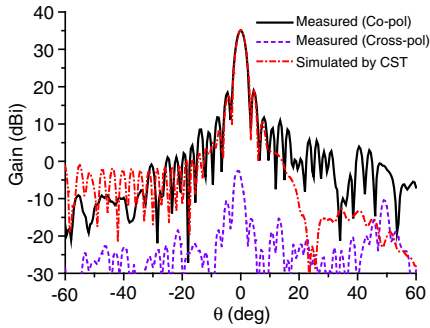**Figure 10.** Comparison of the simulated gain patterns for SLA and HLA (12.5 GHz).

Figure 11. Comparison of the simulated and measured gain patterns of the HLA (12.5 GHz).
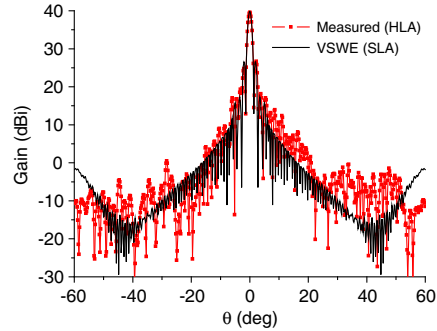
Figure 12. Comparison of the simulated and measured gain patterns for HLA and SLA (30 GHz).

HLA and SLA are superimposed at main lobe and main sidelobes, as shown in Figure 10. The gain of SLA for 12.5 GHz is 35.4 dBi, while the corresponding result of HLA is 35.21 dBi. Actually, it is also suitable for other high elevation angles.

Since the dimension of the HLA is too large to be measured by far-field system in our anechoic chamber, it was measured using a planar near-field measurement system (Figure 8). The primary property of probing the near-field on a finite planar surface to calculate the far-field is that the resulting far-field pattern is over a limited angular span (max angle $< \pm 70°$). Figure 11 and Figure 12 illustrate the comparison of the simulated and measured gain patterns of the HLA at 12.5 GHz and 30 GHz, respectively. Due to the limitation of our computer, the full wave simulated gain pattern at 30 GHz is not available. Thus, only the gain pattern of SLA simulated by VSWE is provided. The simulated gain results of SLA are 35.4 dBi and 39.84 dBic at 12.5 GHz and 30 GHz, respectively. The corresponding measurement results of HLA are 35.07 dBi and 39.61 dBic, respectively. The measured sidelobe levels of HLA are -16.2 dB and -13.0 dB at 12.5 GHz and 30 GHz, respectively. The measured cross polarization isolation is about 38 dB at 12.5 GHz, and the axial ratio is less than 2.8 dB at 30 GHz. Some disagreements (Figure 11) occur at the right-side sidelobe region may be caused by blockage of the feed and supporting struts during the measurement. Nevertheless, the agreements between measured results and simulated results are reasonable.

The feed-to-lens distance is an important aspect in designing SLAs. In practice, the feed of an SLA is usually an aperture antenna, and a suitable feed-to-lens distance should be properly
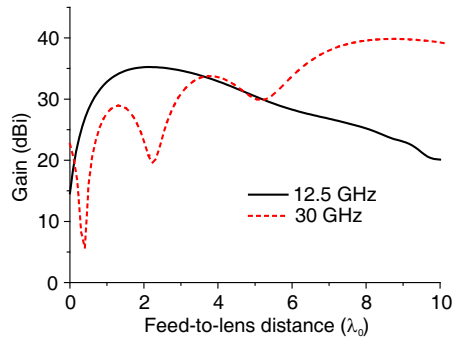
Figure 13. Influence of the feed-to-lens distance f on the gain of SLA.

selected to obtain a compromise between the spillover efficiency and taper efficiency. Figure 13 shows the influence of feed-to-lens distance f on the gain of SLA. The gain for 30 GHz is sensitive to variations of the location of feed, yet for 12.5 GHz the gain profile changes slowly. The SLA has optimal gain for $f_{\mathrm{ku}} = 57\,\mathrm{mm}$ and $f_{\mathrm{ka}} = 86\,\mathrm{mm}$. The designed SLA with defocused source gives rise to aperture phase errors. Due to the electrically large size SLA (about 65λ diameter, especially at 30 GHz) with a smallest number of layers, there is a focal domain outside of the lens. When the phase center of the feed moves within this domain, the aperture phase distribution of the lens performs uniformly in some areas and changes dramatically in other areas. That is why the gain for 30 GHz is fluctuating in the focal domain.

4. CONCLUSIONS

This paper presents an integrated strategy for the optimal design of an electrically-large size SLA including PFM with a smaller layers. The VSWE combined with DE algorithm is adopted to fulfill this target, and the full-wave simulated aperture near-field distributions of feeds are also taken into account in the DE optimization procedure. The performances of the optimized 2-layer design are compared with previous works, higher directivity is obtained. A 650 mm diameter 2-layer SLA is presented to validate the approach. The convergence performance of DE algorithm for the SLA is also investigated. Finally, the choices of the various lens-to-feed distances and aperture sizes of 2-layer SLA for the desired optimum radiation characteristics are also proposed. The study shows that the proposed method can precisely describe the radiation characteristics of the entire lens-feed antenna system and also provide design guidelines of the feed.

ACKNOWLEDGMENT

REFERENCES

1. Liang, C. S., D. A. Streater, J.-M. Jin, E. Dunn, and T. Rozendal, "A quantitative study of luneberg-lens reflectors," *IEEE Antennas Propag. Mag.*, Vol. 47, No. 2, 30–41, 2005.

2. Vinogradov, S. S., P. D. Smith, J. S. Kot, and N. Nikolic, "Radar cross-section studies of spherical lens reflectors," *Progress In Electromagnetics Research*, Vol. 72, 325–337, 2007.

3. Nikolic, N., J. S. Kot, and S. Vinogradov, "Scattering by a Luneberg lens partially covered by a metallic cap," *Journal of Electromagnetic Waves and Applications*, Vol. 21, No. 4, 549–563, 2007.

4. Schrank, H. and J. Sanford, "A Luneberg-lens update," *IEEE Antennas Propag. Mag.*, Vol. 37, No. 1, 76–79, Feb. 1995.

5. Schoenlinner, B., X. Wu, J. P. Ebling, G. V. Eleftheriades, and G. M. Rebeiz, "Wide-scan spherical-lens antennas for automotive radars," *IEEE Trans. Microwave Theory Tech.*, Vol. 50, No. 9, 2166–2175, Sep. 2002.

6. Dou, W. B., Z. L. Sun, and X. Q. Tan, "Fields in the focal space of symmetrical hyperbolic focusing lens," *Progress In Electromagnetics Research*, Vol. 20, 213–226, 1998.

7. Thakur, J. P., W.-G. Kim, and Y.-H. Kim, "Large aperture low aberration aspheric dielectric lens antenna for W-band quasi-optics," *Progress In Electromagnetics Research*, Vol. 103, 57–65, 2010.

8. Sun, F. and S. He, "Can Maxwell's fish eye lens really give perfect imaging?" *Progress In Electromagnetics Research*, Vol. 108, 307–322, 2010.

9. Sun, F., X. Ge, and S. He, "Can Maxwell's fish eye lens really give perfect imaging? Part II. The case with passive drains," *Progress In Electromagnetics Research*, Vol. 110, 313–328, 2010.

10. Zhong, M., S. Yang, and Z. Nie, "Optimization of a Luneberg lens antenna using the differential evolution algorithm," *Proc. IEEE AP-S Int. Symp. Dig.*, San Diego, CA, Jul. 2008.

11. Stratton, J. A., *Electromagnetic Theory*, 204–207, McGraw Hill, New York, 1941.

12. Tai, C. T., "The electromagnetic theory of the spherical Luneberg lens," *Appl. Sci. Res.*, Section B, Vol. 7, 113–130, 1958.

13. Sanford, J. R., "Scattering by spherically stratified microwave lens antennas," *IEEE Trans. Antennas Propag.*, Vol. 42, No. 5, 690–698, May 1994.

14. Mosallaei, H. and Y. Rahmat-Samii, "Non-uniform Luneburg and two-shell lens antennas: Radiation characteristics and design optimization," *IEEE Trans. Antennas Propag.*, Vol. 49, No. 1, 60–69, Jan. 2001.

15. Thornton, J., "Wide-scanning multi-layer hemisphere lens antenna for Ka band," *IEE Proc.-Microw. Antennas Propag.*, Vol. 153, No. 6, 573–578, 2006.

16. Fuchs, B., R. Golubovic, A. K. Skrivervik, and J. R. Mosig, "Spherical lens antenna designs with particle swarm optimization," *Microw. Opt. Techn. Lett.*, Vol. 52, No. 7, 1655–1659, Jul. 2010.

17. Fuchs, B., S. Palud, L. Le Coq, O. Lafond, M. Himdi, and S. Rondineau, "Scattering of spherically and hemispherically stratified Lenses fed by any real source," *IEEE Trans. Antennas Propag.*, Vol. 56, No. 2, 450–460, Feb. 2008.

18. Peeler, G. D. M. and H. P. Coleman, "Microwave stepped-index Luneberg lenses," *IEEE Trans. Antennas Propag.*, Vol. 6, No. 2, 202–207, 1958.

19. Carpenter, Michael, P., et al., "Lens of gradient dielectric constant and methods of production," U. S. Patent 6-433-936 B1, 2001.

20. Rondineau, S., M. Himdi, and J. Sorieux, "A sliced spherical Lüneburg lens," *IEEE Antennas Wireless Propag. Lett.*, Vol. 2, 163–166, 2003.

21. Ma, H. F., X. Chen, H. S. Xu, X. M. Yang, W. X. Jiang, and T.-J. Cui, "Experiments on high-performance beam-scanning antennas made of gradient-index metamaterials," *Appl. Phys. Lett.*, Vol. 95, 094107, 2009.

22. Ma, H. F., X. Chen, X. M. Yang, W. X. Jiang, and T.-J. Cui, "Design of multibeam scanning antennas with high gains and low sidelobes using gradient-index metamaterials," *J. Appl. Phys.*, Vol. 107, 014902, 2010.

23. Wang, G., Y. Gong, and H. Wang, "On the size of left-handed material lens for near-field target detection by focus scanning," *Progress In Electromagnetics Research*, Vol. 87, 345–361, 2008.

24. Andrés-García, B., L. E. García-Muñoz, V. Gonzalez-Posadas, F. J. Herraiz-Martínez, and D. Segovia-Vargas, "Filtering lens structure based on SRRs in the low THz band," *Progress In Electromagnetics Research*, Vol. 93, 71–90, 2009.

25. Agastra, E., G. Bellaveglia, L. Lucci, R. Nesti, G. Pelosi, G. Ruggerini, and S. Selleri, "Genetic algorithm optimization of high-efficiency wide-band multimodal square horns for discrete lenses," *Progress In Electromagnetics Research*, Vol. 83, 335–352, 2008.

26. Hosseini, S. A. and Z. Atlasbaf, "Optimization of side lobe level and fixing quasi-nulls in both of the sum and difference patterns by using continuous Ant Colony Optimization (ACO) method," *Progress In Electromagnetics Research*, Vol. 79, 321–337, 2008.

27. Storn, R. and M. Siemens AG, "On the usage of differential evolution for function optimization," *Biennial Conference of the North American*, 519–523, 1996.

28. Qing, A., "Electromagnetic inverse scattering of multiple two-dimensional perfectly conducting objects by the differential evolution strategy," *IEEE Trans. Antennas Propag.*, Vol. 51, 1251–1262, 2003.

29. Yang S., Y. B. Gan, and A. Qing, "Antenna-array pattern nulling using a differential evolution algorithm," *Int. J. RF Microwave Comput. Aided Eng.*, Vol. 14, No. 1, 57–63, 2004.

30. Li, J.-Y. and J. L. Guo, "Optimization technique using differential evolution for Yagi-Uda antennas," *Journal of Electromagnetic Waves and Applications*, Vol. 23, No. 4, 449–461, 2009.

31. Li, G., S. Yang, M. Huang, and Z. Nie, "Sidelobe suppression in time modulated linear arrays with unequal element spacing," *Journal of Electromagnetic Waves and Applications*, Vol. 24, Nos. 5–6, 775–783, 2010.